Gamma rays and energetic particles from primordial black holes

F. Halzen, E. Zas, J. H. MacGibbon & T. C. Weekes

Black holes of almost arbitrarily small mass may have formed in the very early Universe. Their presence today would be revealed by the energetic radiation they would produce by means of the quantum-gravitational Hawking mechanism, allowing observational limits to be set on their density today and on their past significance.

UNDER present cosmic conditions, black holes can form only by self-gravitational collapse, and since masses of about three solar masses ($M_\odot$) or less are stable when cold in the form of neutron stars or white dwarfs, modern black holes must exceed a few $M_\odot$ in mass. But in the early Universe primordial black holes (PBHs) of almost arbitrarily small mass may have formed. The simplest mechanism[1,2] is the collapse of overdense regions in a universe with significant density fluctuations; the resulting PBHs have masses roughly equal to the mass contained within the cosmic horizon (essentially c times the age of the Universe), which can be as low as the Planck mass $(hc/G)^{1/2} \approx 5 \times 10^{-11}$ g. More exotic formation mechanisms include cosmic phase transitions[3] or the collapse of loops of cosmic string[4,5]. The presence of any such PBHs in the Universe today would go largely unnoticed were it not for the Hawking radiation from black holes[6], a phenomenon arising out of the union of general relativity and quantum mechanics, according to which black holes can radiate particles whose Compton wavelength is less than the Schwarzschild radius of the black hole (see Box 1).

For black holes of solar-mass size, Hawking radiation is quite negligible, but for small enough PBHs, it becomes the controlling influence in the black hole's evolution. PBHs of $\sim 5 \times 10^{14}$ g or less will indeed have evaporated entirely in the 10^{10} years or so of the Universe's history. PBHs a little more massive than this initially will still be evaporating, at a rate large enough that the stream of energetic particles and radiation they emit can be turned into a strong observational limit on their presence. The cosmic ray and γ-ray backgrounds place an upper limit on the integrated density of PBHs with initial masses in this range of $\sim 10^{-8} \rho_c$, where ρ_c is the critical density required to close the Universe, but even at this level their emissions could make a significant contribution to the observed extragalactic γ-ray and interstellar positron, electron and antiproton backgrounds. PBHs whose initial mass exceeded 5×10^{14} g by two orders of magnitude or more can provide ρ_c but escape detection because their emission would be concealed by the larger observed backgrounds at energies of 100 keV or less.

Moreover, a population of PBHs whose influence is small today may have been more important earlier in cosmic history. Too much radiation from PBHs could perturb the usual picture of cosmological nucleosynthesis[7], distort the microwave background[8] and produce too much entropy in relation to the matter density of the Universe (for a recent review, see ref. 9). In general, limits on the density of PBHs, now or at earlier times, can be used to provide information on the homogeneity and isotropy of the very early Universe, when they were formed[10].

Searches for PBHs attempt either to detect a diffuse photon background from a distribution of PBHs or to search directly for the final emission stage of individual holes. Here we review the status of the search for PBHs and discuss strategies for improving the existing bounds on black-hole abundance, obtained from diffuse megaelectronvolt γ-ray data[11,12], by exploiting air-shower telescopes to search for the final γ-ray emission. Particle emission by PBHs was initially researched over a decade ago[6,10,11] and has been recently reconsidered by MacGibbon, Carr and Webber[12–14] in light of the discovery of the quark–lepton structure of matter. They assume that asymptotically free quarks and gluons are emitted which hadronize into jets of astrophysically stable photons, neutrinos, electrons, positrons, protons and antiprotons. The jet emission mimics particle production by an electron–positron collider. The ultimate behaviour of a black hole at very high temperatures is particularly interesting, as it is dictated by particle physics beyond the range of current particle accelerators. We will calculate the experimental signatures of Hawking radiation in the

BOX 1 Hawking radiation from black holes

The radiation of particles by black holes can be qualitatively understood by analogy with the production of e^+e^- pairs in the presence of strong electric fields. In quantum mechanics, virtual e^+e^- are continuously created and destroyed in the vacuum. A strong field can separate the charges, and as a result, particles can tunnel through the quantum barrier and pop out of the vacuum as real particles. The threshold field strength is given by

$$eE\lambda > 2m_e c^2 \tag{1}$$

The left-hand side is the work done in separating the particles by a Compton wavelength λ. The right-hand side is the energy required to create the particles. The energy of the particles can be estimated as follows

$$E = kT \propto pc \propto \frac{\hbar}{\lambda} c \propto \frac{\hbar c^3}{2G} M^{-1} \tag{2}$$

where we took the horizon or Schwarzschild radius of the black hole $2GM/c^2$ as the relevant Compton wavelength. The luminosity is determined by the area multiplied by the energy

$$L \equiv \frac{dM}{dt} = (4\pi\lambda^2)(aT^4) \propto M^{-2} \tag{3}$$

The energy is determined by the Stefan–Boltzman relation and the proportionality constant, a, in (3) therefore contains the number of degrees of freedom of the particle emitted. The timescale associated with this radiation is

$$t = \frac{M}{dM/dt} \propto M^3 \tag{4}$$

These dimensional estimates can be summarized as follows

$$T \approx 100\ \text{MeV} \left(\frac{10^{15}\ \text{g}}{M}\right) \tag{5}$$

$$L = 10^{20}\ \text{erg s}^{-1} \left(\frac{10^{15}\ \text{g}}{M}\right)^{-2} \tag{6}$$

$$t \approx 10^{10}\ \text{yr} \left(\frac{M}{10^{15}\ \text{g}}\right)^3 \tag{7}$$

Small black holes with mass of $\lesssim 10^{15}$ g or less should be observable. They are characterized by high temperatures and luminosities. They moreover have lifetimes such that they evaporate, possibly explosively, within the lifetime of the universe.

context of the standard model of quarks and leptons and also illustrate the effect of particle degrees of freedom beyond the standard model. The standard model is known to be incomplete, and the additional degrees of freedom are a subject of intense speculation. Searching for them constitutes the primary mission of future accelerators such as the SSC.

On the experimental side, a new generation of particle detectors, covering the TeV (10^{12} eV) and PeV (10^{15} eV) energy ranges, and new γ-ray telescopes such as the EGRET detector on the Gamma Ray Observatory greatly increase the potential sensitivity of searches for Hawking radiation (Box 2). The astronomical activity of such instruments has almost exclusively been focused on the search for point sources of ultra-energetic particles[15-18]. These detectors can probe diffuse high-energy photon backgrounds produced by galactic and extragalactic cosmic rays[19,20]. Here we emphasize another measurement of cosmological relevance, namely the search for Hawking radiation from black holes.

BOX 2 TeV- and PeV-astronomy

The predicted fluxes of TeV and PeV cosmic photons are smaller than the cosmic ray flux in the corresponding energy range. The photons are absorbed by the atmosphere, and detectors of area ~1 m^2 carried by rockets or satellites are not sensitive to the small fluxes discussed here. Fortunately the same atmosphere that shields the photons from Earth constitutes a calorimeter medium which can be exploited to detect them. The atmosphere represents a layer of material with a column density of 1,000 g cm^{-2}, corresponding to ~25 radiation lengths. The primary photons initiate showers which dissipate their energy into a vast number of electrons and photons, which are absorbed by the atmosphere at a height of ~10 km. Only the energy dissipated in weakly interacting neutrinos and muons, which are the decay products of pions photoproduced in the cascades, penetrates to observation level on a mountain top or at sea level. Muons lose 2 MeV of their energy through ionization for every 1 g cm^{-2} of matter traversed. To penetrate 1,000 g of atmosphere they must have started with at least 2 GeV energy, and a parent primary must have an energy of at least 10 GeV to be detected via sea-level muons.

The showers initiated by cosmic photons with energies exceeding 100 TeV have a lateral spread of ~0.1–1 km, because the secondary particles diverge as a result of their transverse momentum and secondary interactions in the atmosphere. An 'extensive air-shower array' of, say, 100 m^2 can detect showers over an effective area of 10 km^2, a gain in sensitivity of 10^5, because only a fraction of the shower must traverse the array of detectors to be detected. The trajectory of the primary particle need not be contained inside the array. The array itself can consist of relatively widely separated particle detectors (usually a scintillator viewed by a phototube) sampling the 100-m^2 area. Enough particles survive to mountain (sea-level) altitudes for showers of 10 (100) TeV primary energy to be detected in this way.

Another technique consists of using mirrors viewed by phototubes collecting the Čerenkov light produced by shower particles in the atmosphere. Showers with energies as low as 0.1 TeV can be detected using this technique. A 100-GeV shower still produces several hundred electrons at an altitude of 10 km. A mirror with 2° aperture views showers over an effective area of 10^5 m^2 at an altitude of 10 km on a mountain. Recent experiments have been successful in distinguishing the γ-ray showers from the much more numerous proton showers on the basis of the size of the Čerenkov light image.

At higher energies a popular technique is to measure the electromagnetic and muon component simultaneously in a single shower. The muon detector can be a GeV-muon detector at or near the surface, or a deep underground TeV-muon detector triggered by the air-shower array. The simultaneous determination of the number of electrons and muons in the cascade could lead to the determination of the nature of the primary particle—that is, whether it is a proton or a heavy nucleus. Another possibility to be explored with such a hybrid detector is to do γ-ray astronomy in the presence of cosmic-ray backgrounds by selecting showers poor in muons. Reduced pion production in a photon cascade leads us to expect that the number of muons in a photon shower is less than 5% of the number in a proton shower with similar energy or similar number of electrons[36]. Muon-poor astronomy therefore requires measurement of the muon and electron number in each individual shower.

Hawking radiation and emission models

Hawking showed that an uncharged, non-rotating black hole emits particles with energy in the range $(E, E+dE)$ at a rate[16]

$$\frac{d^2N}{dt\,dE}=\frac{\Gamma_s}{2\pi\hbar}\left[\exp\left(\frac{8\pi GME}{\hbar c^3}\right)-(-1)^{2s}\right]^{-1} \quad (1)$$

per state of angular momentum and spin. Here M is the mass of the hole, s is the particle spin, and Γ_s, the absorption coefficient, is in general a function of s, E and M (ref. 21). The absorption coefficient is the probability that the particle would be absorbed if it were incident in this state on the black hole. It appears in the emission formula on account of detailed balance between emission and absorption. In the limit $ME \gg 1$, the instantaneous emission is a function of ME only and the spectrum is that of a black body with a temperature of

$$T \approx 1.06\times10^{13}\left[\frac{1\text{ g}}{M}\right]\text{ GeV} \quad (2)$$

The instantaneous photon flux peaks at $ME \approx 6.12\times10^{13}$ g GeV. Integrated over all energies, the photon flux is

$$dN/dt = 5.97\times10^{34}\left[\frac{1\text{ g}}{M}\right]s^{-1} \quad (3)$$

The instantaneous flux of electrons and positrons peaks at a 50% higher value of ME and the integrated combined $e^{\pm}$ flux is a factor of 6–7 larger than the photon flux. The detailed spectra, which we will use as input into calculations throughout this review, have been calculated by Page[21,22] for spin-$\frac{1}{2}$ and spin-1 particles, and by Elster[23,24] and Simpkins[25] for spin-0 particles.

The black hole loses mass at a rate[21]

$$\frac{dM}{dt}=-\frac{\alpha(M)}{M^2} \quad (4)$$

where $\alpha(M)$ accounts for the degrees of freedom of each emitted particle contributing to the energy loss. As the hole radiates, its temperature rises and α increases smoothly at the rest-mass threshold for each new massive particle (Fig. 1). Above each threshold, α is approximately

$$\alpha \approx [7.8d_{s=1/2}+3.1d_{s=1}]\times10^{24}\text{ g}^3\text{ s}^{-1} \quad (5)$$

where $d_{s=1/2}$ and $d_{s=1}$ are the number of degrees of freedom (spin, charge and colour) of the emitted particles. For the standard model with three fermionic generations, we have $d_{s=1}=27$ and $d_{s=1/2}=90$ at $T\approx100$ Gev, and so $\alpha \geq 7.8\times10^{26}$ g^3 s^{-1} (if we ignore the contributions from the Higgs scalars and gravitons, which have not yet been confirmed experimentally).

Not only does the standard model dictate the high-energy behaviour of the hole, but quantum chromodynamics (QCD) modifies the flux calculations above ~100 MeV. Quarks and gluons, rather than pions and heavier hadrons, should be emitted once the temperature of the black hole (or the peak in the flux distribution) exceeds the quark-gluon deconfinement temperature $\Lambda_{qh}\approx100$–300 MeV. Of the hadrons, only pions will be directly emitted below Λ_{qh}. This, of course, only occurs if Λ_{qh}, whose value is not accurately known, exceeds the rest mass of the pion. The emission can be understood by analogy with hadron production in e^+e^- collisions. A virtual photon, produced at rest by e^+ and e^- beams colliding head on, can decay into a quark–antiquark pair. When the pair separate by a distance of ~1 Fermi (10^{-15} m), the colour interactions between the quarks become exceedingly strong, and violent forces decelerate the quarks. As a result they radiate hadrons (mostly light pions) just as a decelerated charge emits photons by bremsstrahlung. The original quark is never seen; only a 'jet' of pions and other colourless hadrons hits the detector. Similarly a Fermi-size black hole will initially radiate quarks once their energy exceeds Λ_{qh}. The time between emissions is short enough so that we can

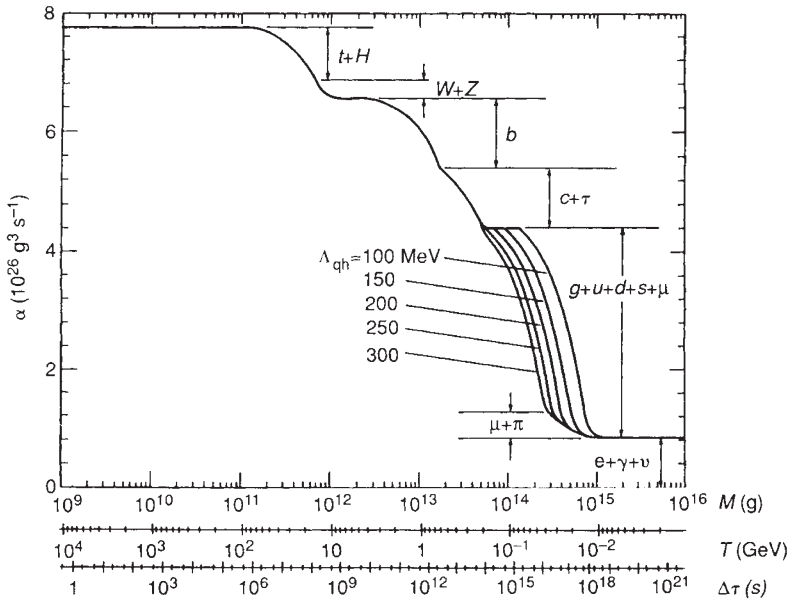

FIG. 1 The parameter α counting the degrees of freedom of the Hawking mass radiation as a function of the black-hole temperature and lifetime. Λ_{qh} is the quark–hadron deconfinement scale. The contribution from each particle species is indicated.

neglect interactions between successive emissions before fragmentation into pions occurs[13,26]. The emitted quarks and gluons can therefore be treated as asymptotically free partons hadronizing to produce jets of pions far beyond the black hole horizon. This is analogous to the production of jets in e^+e^- annihilation. These jets are described by empirical fragmentation functions which represent the way in which the momentum of an initial quark or gluon is distributed among the fragmenting hadrons. These fragmentation functions can be calculated from convenient parametrizations of accelerator data or by Monte Carlo techniques based on QCD[13].

In this picture it is straightforward to convolve equation (1), describing the emission of quarks and gluons, with the empirical fragmentation functions to obtain the instantaneous emission spectra. In the astrophysical case, the pions will decay into stable $e^{\pm}$, γ and $\nu\bar{\nu}$. The jets will also produce protons and antiprotons. The black hole also emits direct $e^{\pm}$, γ and $\nu\bar{\nu}$ fluxes as in equation (1). As an illustration, we show in Fig. 2 the total particle fluxes radiated by a black hole of temperature $T=10$ GeV. The photon spectrum has a dominant peak around 100 MeV coming from jet pion decays and a smaller bump at an energy of $\sim 5T$ coming from direct γ-ray emission. The β-decay of jet neutrons produces low-energy bumps in the lepton spectra around 1 MeV.

The value of α in equation (5) represents a minimum bound at energies exceeding those probed by particle accelerators. For example, if supersymmetry is the underlying theory for high-energy elementary particles, α should increase by at least a factor of three. There have been many speculations on physics beyond the standard model. We will resist the temptation of listing their predictions and instead choose an extreme example[27,28] where the number of degrees of freedom grows exponentially with mass, m

$$N \approx m^{-5/2} \exp\left[\frac{m}{\Lambda}\right] \qquad (6)$$

The Hagedorn picture, which is motivated by the apparent exponential increase in hadronic resonances, is an example of such a theory. Although not favoured, it is not yet ruled out by particle physics experiments and has been recently revived in the context of string theories at the Grand Unified Theory scale. An exponentially growing density of states causes the final explosion of the black hole to be much more violent. Once a limiting temperature is reached, the remaining mass is suddenly emitted into all available states. This occurs when the exponential increase in the number of states offsets the exponential decrease in the tail of the Hawking radiation at a critical black-hole mass of $M_c = (1.06\times10^{13}\ \text{GeV})/\Lambda$ g. More realistically, equations of the form of equation (6) may indicate that a phase transition, whose details are as yet unknown, occurs at Λ. In this case, the quasi-exponential spectrum would not continue until $m\to\infty$ but would last for, at most, the duration of the finite phase transition. Again we could observe bursts carrying off a significant fraction of the PBH's mass from holes just reaching the phase transition temperature. In the final section, we shall calculate the chance of detecting the final evaporation stage both for a Hagedorn scheme with $\Lambda = 160$ MeV and for the standard model. These cases represent two extreme extrapolations of the particle model.

Diffuse backgrounds from Hawking radiation

By integrating equation (4), one can relate[21] the initial mass M_i of the black hole to its lifetime, that is, the time, τ_{evap}, over which it completely evaporates. To a good approximation we have

$$M_i \approx [3\alpha(M_i)\tau_{evap}]^{1/3} \approx 5.4\times10^8\left[\frac{\alpha(M_i)}{5.3\times10^{25}\ \text{g}^3\ \text{s}^{-1}}\right]^{1/3}\left[\frac{\tau_{evap}}{1\ \text{s}}\right]^{1/3}\text{g} \qquad (7)$$

A hole that formed in the early Universe and is just completing its evaporation today therefore had an initial mass $M_* \approx [3\alpha(M_*)t_0]^{1/3}$ where t_0 is the age of the Universe. In Friedman models, t_0 depends on the relative matter density Ω_m and the Hubble constant $H_0 = h_0/100\ \text{km s}^{-1}\ \text{Mpc}^{-1}$. Because M_* is close to the thresholds for $\mu^{\pm}$, $\pi^{0,\pm}$ and u, d quark emission, we integrate equation (4) and solve numerically for M_* by approximating α linearly at each threshold[29]. We find that M_* lies in the range[14]

$$4.3\times10^{14} < M_* < 7.0\times10^{14}\ \text{g} \qquad (8)$$

for $125 \leqslant \Lambda_{qh} \leqslant 300$ MeV, $0.06 \leqslant \Omega_m \leqslant 1.0$ and $0.4 < h_0 < 1$. As $\tau_{evap} \propto M_i^3$, black holes with $M_i \gg M_*$ have not lost a significant amount of mass by today, whereas those with $M_i < M_*$ have completely evaporated.

PBHs could have formed in the early Universe in a number of ways[1]. They may, for example, have been produced by initial density inhomogeneities[2] or as a result of a phase transition[3]. Hawking, Zembowicz and Polnarev have also recently proposed that a spectrum of black holes may have been created by the collapse of cosmic strings[4,5]. If spherically symmetric PBHs form from scale-invariant initial density perturbations that have a

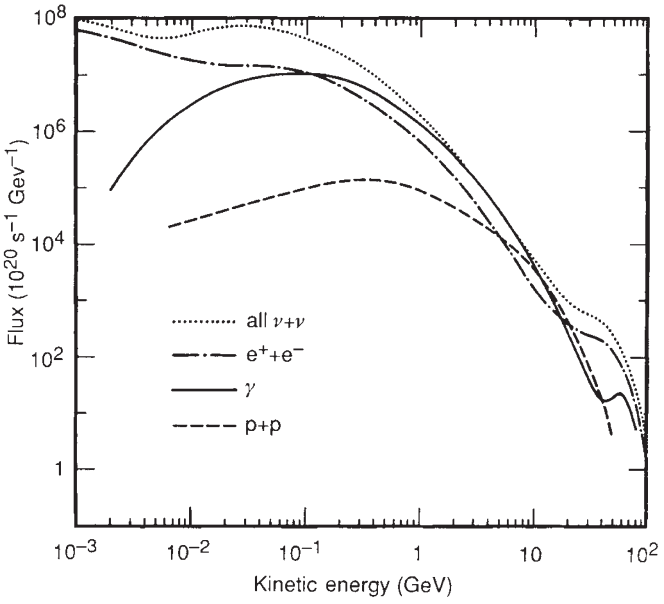

FIG. 2 Particle fluxes radiated by a black hole of temperature $T = 10$ GeV.

gaussian distribution, the number density of holes created with mass in the range $(M_i, M_i + dM_i)$ is[30]:

$$\frac{dn}{dM_i} = \frac{\mathcal{N}}{M_*}\left[\frac{M_i}{M_*}\right]^{-\beta} \tag{9}$$

Here $\mathcal{N} = (\beta - 2)\Omega_{PBH}\rho_c / M_*$, where Ω_{PBH} is the present fraction of the cosmological critical mass density ρ_c in holes of $M \geq M_*$. $\mathcal{N}$ corresponds to the initial number density of holes per logarithmic mass interval at $M = M_*$. If the equation of state of the Universe is $p = \gamma\rho$ at the formation epoch, where p is pressure, then $\beta = (1 + 3\gamma)/(1 + \gamma) + 1$. For PBHs forming in the radiation-dominated era, we have $\beta = 2.5$.

The emission from PBHs over the lifetime of the Universe will produce diffuse particle backgrounds. These can be compared with observations to obtain an upper limit[11] on Ω_{PBH} and hence $\mathcal{N}$. The predicted diffuse photon spectrum is shown in Fig. 3 for the initial distribution equation (9) with $\beta = 2.5$. We have included quark and gluon emission and neglected all losses other than redshift. The integrated emission[29] shown in Fig. 3 has an E^{-1} slope for photon energies well below 100–300 MeV, coming from jet fragmentation, and turns over into an E^{-3} slope above 300 MeV. The E^{-3} slope, which is independent of the value of β, is dominated by direct photon emission and comes from evaporation in the present epoch. Matching to the observed γ-ray spectrum at 100 MeV (where photon losses are negligible), as was done in Fig. 3, yields a bound on the density of PBHs[12]

$$\Omega_{pbh} \leq 7.6(\pm 2.6) \times 10^{-9} h_0^{-1.95 \pm 0.15} \tag{10}$$

for $\Omega_m = 1.0$ and $\beta = 2.5$. This corresponds to $\mathcal{N} \leq 10^4\ \mathrm{pc}^{-3}$. The limit is ~60% weaker for $\Omega_m = 0.06$ and varies by ≤50% when the value of Λ_{qh} is changed. MacGibbon and Carr[12] also obtain bounds on Ω_{pbh} from the antiproton, electron and positron fluxes. These bounds are remarkably similar to the γ-ray limit (equation (10)) if the PBHs are clustered to the same degree as other material in the galactic halo. (In this case, the local density is enhanced by a large factor which we estimate below to be in excess of 10^7.) The bounds may even overlap, allowing the possibility that PBH emission may be contributing significantly to all observed interstellar cosmic ray and γ-ray spectra between 0.1 and 1 GeV. It should be pointed out that none of these conclusions depend sensitively on the initial distribution (equation (9)). The limit given in equation (10) is always valid, as it is essentially determined by the peak emission from the holes with critical mass M_* (see equation (3)).

From the initial PBH distribution, we can calculate the distribution of holes at any later time t. If we invoke equation (7), the distribution of equation (9) becomes[10]

$$\begin{aligned}\frac{dn}{dM} &= \frac{dn}{dM_i}\frac{dM_i}{dM} \\ &\approx \frac{\mathcal{N}}{M_*}\left[1 + \left(\frac{t}{t_0}\right)\left(\frac{\alpha(M)}{\alpha(M_*)}\right)\left(\frac{M}{M_*}\right)^{-3}\right]^{-(\beta+2)/3} \\ &\quad \times \left[\frac{M}{M_*}\right]^{-\beta}\left[\frac{\alpha(M)}{\alpha(M_i)}\right]^{(\beta-1)/3} \\ &\propto \begin{cases} M^2, & M \ll 10^9 t^{1/3}\ \mathrm{g} \\ M^{-\beta}, & M \gg 10^9 t^{1/3}\ \mathrm{g} \end{cases}\end{aligned} \tag{11}$$

where M is the mass at time t of a hole with initial mass M_i. Note that the present distribution for $M \ll M_*$ is independent of β. Regardless of their formation mechanism, holes today with masses less than M_* have the distribution $dn/dM \propto M^2$. From equation (11), or directly from equation (4), we now obtain the current rate of expiring PBHs,

$$\frac{dn}{dt} = \frac{\alpha(M_*)}{M_*^3}\mathcal{N} \approx \frac{\mathcal{N}}{t_0} \tag{12}$$

Allowing for uncertainties in M_* and $\alpha(M_*)$, the present rate of explosions averaged over the Universe should thus lie in the range

$$\begin{aligned} &1.2 \times 10^{-11}\ \mathrm{yr}^{-1}\ (h_0 = 0.4) \\ &< \frac{dn}{dt}\mathcal{N}^{-1} \\ &< 4.0 \times 10^{-11}\ yr^{-1}\ (h_0 = 1.0) \end{aligned} \tag{13}$$

As they should not have large peculiar velocities, one should expect PBHs to cluster in galactic haloes along with other material. This will enhance their local density by a factor ζ. Assuming an isothermal halo we estimate[2] a local enhancement factor at $R_\odot$, the Sun's distance from the Galactic Centre, of

$$\zeta = 1.36(\pm 0.9) \times 10^7 \left(\frac{\Omega_\odot}{0.01}\right)^{-1} h_0^{-2} \tag{14}$$

where $\Omega_\odot$ is the visible fraction of ρ_c in galaxies out to $R_\odot$. A detailed discussion will be given elsewhere (F.H., J.H.M., T.C.W. and E.Z., manuscript in preparation). The large uncertainties associated with clustering will strongly affect our chances for detecting PBH evaporations. For $\mathcal{N} = 10^4\ \mathrm{pc}^{-3}$, the present local rate of explosions could be as low as $10^{-7}\ \mathrm{pc}^{-3}\ \mathrm{yr}^{-1}$, if holes are not clustered, or as high as $10\ \mathrm{pc}^{-3}\ \mathrm{yr}^{-1}$ if holes are clustered. As γ-rays (unlike charged particles) are not confined in the Galaxy, the diffuse photon background from PBHs is not affected by clustering.

Final-stage emission

The final radiation from a black hole is dictated by particle physics. We will first assume the degrees of freedom of the particle to be those of the standard model, even at very high temperatures. Let us consider a black hole of mass M_B which completely evaporates in a time $\Delta\tau$ given by equation (7). Photons are emitted either directly by the Hawking mechanism of equation (3) or as fragmentation products of quarks or gluons (partons). The quark flux, integrated over $\Delta\tau$, peaks at an energy of

$$Q \approx 40\left[\frac{1\ \mathrm{s}}{\Delta\tau}\right]^{1/3}\ \mathrm{TeV} \tag{15}$$

Calculation of the photon flux resulting from fragmentation of these quarks is straightforward and proceeds in three stages:

one starts with the parton fluxes, which fragment into neutral pions, and these then decay into two photons. Here we will follow ref. 31 and choose an empirical fragmentation function of the form $dN_\pi/dz = \frac{15}{16}z^{-3/2}(1-z)^2$, where $z = E_\pi/E_{\rm jet}$.

The predictions relevant to experiment are obtained by integrating the photon flux above a detector threshold $E_{\rm D}$. If the lifetime of the hole is short compared with the observation time, one must integrate its emission spectrum over its history. Assuming that the flux before decay is emitted near the peak energy Q in the Hawking distribution, we find that the time-integrated photon flux from both direct and fragmentation photons decreases as E_γ^{-3} above $E_\gamma \approx Q$. This is a consequence of the time dependence of the hole's temperature given by equations (2) and (7). Below $E_\gamma \approx Q$, the flux traces the slope of the fragmentation function, peaks near the pion mass and is eventually cut off at $E < m_\pi$. Decay photons dominate at all energies, because there are 72 quark and 16 gluon degrees of freedom, but only two direct photon degrees. The contribution per helicity state is also greater for $s = \frac{1}{2}$ than for $s = 1$ states. The number of photons emitted above $E_{\rm D}$ is

$$N_\gamma(>E_{\rm D}) \approx 2.4\times10^{37}\left(\frac{\rm GeV}{Q}\right)^2 \times \begin{cases} \left[\sqrt{\frac{Q}{E_{\rm D}}}\left(\frac{5}{6}+\frac{3E_{\rm D}}{Q}+\frac{5E_{\rm D}^2}{14Q^2}\right)-\frac{5E_{\rm D}}{3Q}-\frac{5}{2}\right]+\frac{1}{250}, & E_{\rm D}<Q \\ \left(\frac{Q}{E_{\rm D}}\right)^2\left[\frac{1}{42}+\frac{1}{150}\left(1-\frac{2}{5}\max\left(0,2-\frac{Q}{E_{\rm D}}\right)\right)\right], & E_{\rm D}\geq Q \end{cases} \quad (16)$$

The direct photons contribute the last terms in these expressions.

Alternatively, if the lifetime is large compared with the observation time, we can freeze the spectrum and calculate the instantaneous flux neglecting the evolution of the hole

$$\frac{dN_\gamma}{dt}(>E_{\rm D}) \approx 8.0\times10^{23}\frac{Q}{1\ {\rm GeV}} \times\left[\frac{1}{4}\left(\frac{Q}{E_{\rm D}}\right)^{1/2}\left(\frac{1+E_{\rm D}^2}{Q^2}\right)-1 +\frac{3}{2}\left(\frac{E_{\rm D}}{Q}\right)^{1/2}-\frac{E_{\rm D}}{Q}\right]{\rm s}^{-1} \quad (17)$$

The detailed structure of the above expressions reflects our choice of fragmentation function.

At energies close to the black-hole temperature, other processes such as prompt photon production may also enhance the flux. The neutrino and co mic-ray emission from the PBHs is comparable to the photonsemission[13]. But as the neutrino and cosmic-ray backgrounds are greater than any postulated diffuse photon background, photon detectors offer the greatest sensitivity to search for individual evaporating PBHs.

Observing isolated black holes

Can the Hawking radiation of an individual hole be detected above the backgrounds created by the distribution of evaporating PBHs or above the observed extragalactic background? If $n_{\rm bh}$ is the local number density of PBHs with present mass less than $M_{\rm th}$, then integration of equation (9) yields

$$n_{\rm bh} \approx \zeta\mathcal{N}\frac{\alpha(M_*)}{3\alpha(M_{\rm th})}\left[\frac{M_{\rm th}}{M_*}\right]^3 \quad (18)$$

for $M_{\rm th} \ll M_*$. According to the mass distribution of equation (18), we expect the closest hole in a volume $n_{\rm bh}^{-1}$ to have an average mass of 0.75 $M_{\rm th}$. The photon flux at the detector from this hole is

$$\frac{d^3N_\gamma}{dA\,dt\,dE_\gamma} = \frac{d^2N_\gamma}{dt\,dE_\gamma}\left[\frac{M_{\rm th}}{M_*}\right]^2\left[\frac{\alpha(M_*)}{\alpha(M_{\rm th})}\right]^{2/3}\frac{\zeta^{2/3}\mathcal{N}^{2/3}}{3\sqrt[3]{12\pi}} \quad (19)$$

where $d^2N_\gamma/dt\,dE_\gamma$ is the instantaneous flux computed for direct photons according to equation (3) and for parton fragmentation photons according to equation (17).

Let us turn first to the diffuse background created by the total emission of all evaporating black holes. Using the results quoted in the previous section, we can represent the PBH background by[29]

$$\frac{d^4N_\gamma}{dA\,dt\,d\omega\,dE_\gamma} \approx 7-14\times10^{-11}\left[\frac{\mathcal{N}}{1\ {\rm pc}^{-3}}\right]E^{-3}\ {\rm cm}^{-2}\,{\rm s}^{-1}\,{\rm sr}^{-1}\,{\rm GeV}^{-1} \quad (20)$$

above 300 MeV, where ω is solid angle, for $0.06 \leq \Omega_m \leq 1.0$, $0.3 \leq h_0 \leq 0.7$ and $\beta = 2.5$. Second, the extragalactic diffuse photon background measured by satellites[33,34,35] between 35 and 170 MeV (ref. 14) is

$$\frac{d^4N_\gamma}{dA\,dt\,d\omega\,dE_\gamma} = 2.7(\pm0.5)\times10^{-4}\left[\frac{E_\gamma}{100\ {\rm MeV}}\right]^{-2.4(\pm0.2)}\ {\rm cm}^{-2}\,{\rm s}^{-1}\,{\rm sr}^{-1}\,{\rm GeV}^{-1} \quad (21)$$

Observations above 170 MeV have not yet been made. The EGRET instrument, recently launched, will be capable of detecting photons up to energies of ~20 GeV. As the galactic emission falls off less steeply than the extragalactic background, however, it is not known if the extragalactic diffuse background can be resolved from the galactic emission above a few hundred MeV, even at high galactic latitude. Regardless of their source, photons with energies $>10^6$ GeV are cut off by pair production on the cosmic microwave background.

To estimate the detector resolution necessary to resolve a point source in the presence of a diffuse background, we require

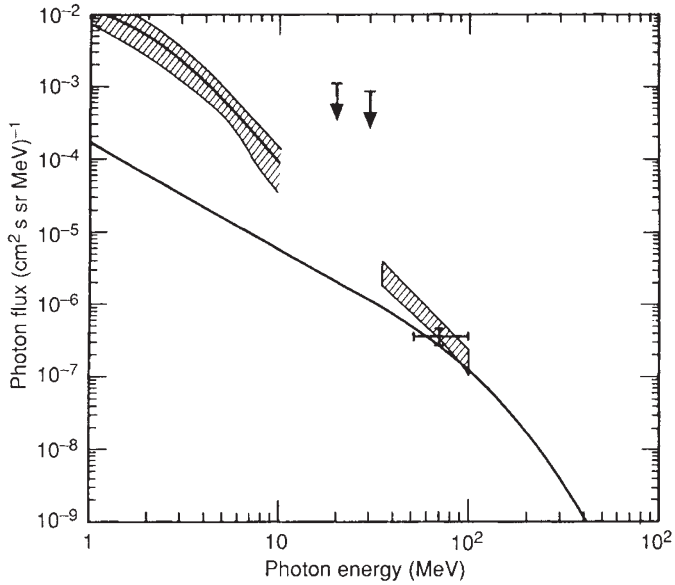

FIG. 3 Diffuse photon flux from Hawking radiation by a distribution of black holes. Shown as a solid line is the calculation for the black-hole density $\Omega_{\rm pbh} = 7.6\times10^{-9}$ leading to the bound in equation (10). Any concentration in excess of this limit would exceed the observed diffuse γ-ray background. Data and upper limits from ref. 28. The hatched areas correspond to 1σ errors.

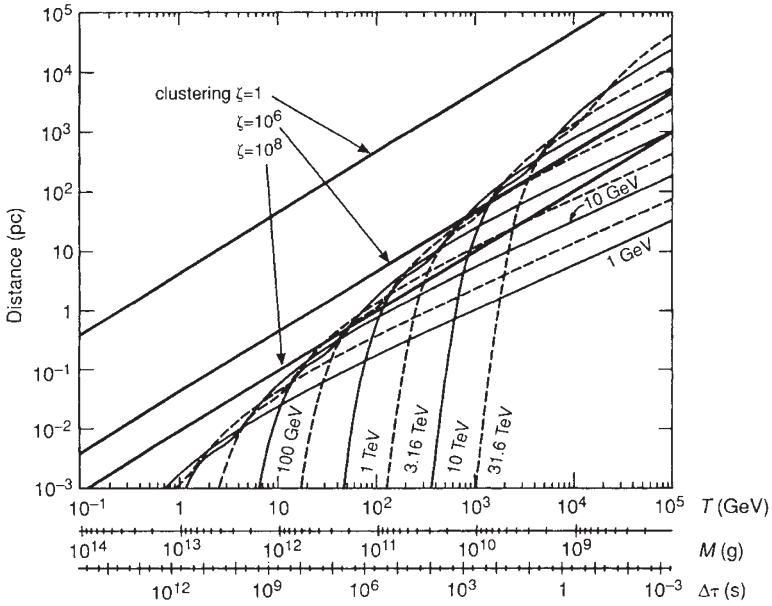

FIG. 4 The three straight lines show the distance at which the closest black hole of temperature $> T$ is expected assuming the maximum density allowed by the bound in Fig. 3. The result is shown for three values of the clustering factor ζ. The other lines show the distance at which the flux from such black hole can be resolved from the diffuse background. Detectors are assumed to have an angular resolution $\omega_D = 10^{-3}$ sr and the energy thresholds shown. The MeV bound in Fig. 3 can be improved by a detector of a given threshold in the region where its sensitivity curve exceeds the straight line.

that the diffuse photon flux within the resolved solid angle of the detector ω_D does not exceed the point source flux; that is,

$$\frac{d^3N_\gamma}{dA\,dt\,dE_\gamma} \geq \omega_D \frac{d^4N_\gamma}{dA\,dt\,d\omega\,dE_\gamma} \qquad (22)$$

As a first example, let us consider the direct photon emission and substitute equations (19) and (20) into (22), assuming $\omega_D = 10^{-3}$ and $\zeta\mathcal{N} \simeq 10^{10}$. In this case we find that black holes of mass $M < 4\times10^{10}$ g and peak photon energy $E_\gamma \simeq (8.66\times10^{13}\text{ g})/M_{th}^{-1}$ GeV will stand out from the PBH background above ~2 TeV. If we compare equation (20) instead with the extrapolation of the measured background, equation (21), the critical energy turns out to be about two orders of magnitude greater. Alternatively, if we look at photon fragments of jets with $E_\gamma/E_{jet} \approx 0.1$, for example, we find that both critical energies are about two orders of magnitude smaller. Thus it may be possible to resolve the instantaneous decay emission from the background at energies above 0.01–1 TeV. This conclusion depends strongly on the nature of the fragmentation function as $E_\gamma/E_{jet} \to 1$ and on the degree to which the PBHs cluster in the galactic halo.

For an estimate more relevant to detectors, we integrate the individual PBH flux above the detector threshold E_D (see equation (16)). Our conclusions are summarized in Fig. 4, which shows the distances at which a hole of temperature T produces a flux in the detector matching the maximum diffuse PBH background allowed by the 100-MeV data. The direct and fragmentation photons produce the bumps at high and low energy, respectively. If the PBHs are clustered with $\mathcal{N}\zeta = 10^{12}$, then detectors with $E_D \geq 30$ GeV may be able to resolve holes of $T \geq 20$ GeV from the background. If $\mathcal{N}\zeta = 10^{10}$, however, the energy threshold for the detector must exceed 300 GeV and the black-hole temperature must exceed 700 GeV. For low temperatures, the detector should see a sky uniformly bright in black holes, and we have a version of Olber's paradox for black holes. In this case, the black-hole horizon is extremely small and the radiation density of the background sky is much smaller than the black-hole surface radiation density. No practical detector can single out a point source because a large number of sources appear in any field of view.

Although the results are model-dependent, the qualitative features illustrated in Fig. 4 should be correct. The distance to the nearest hole of a given temperature should scale as $\zeta^{-1/3}$. The curves shift upward as $\sqrt{10^{-3}/\omega_D}$ with improved detector resolution. Optimum signal-to-noise ratio is obtained at $E_D \approx T$. In Fig. 4, we have used an E^{-3} diffuse background produced by a PBH distribution. If the observed background falls as $E^{-2.4}$, as extrapolated from the MeV data, the conclusions are more restrictive.

At the higher energies, air-shower arrays can search for a diffuse photon background, for example by exploiting the small muon abundance in photon-induced air showers to reject cosmic rays[32]. From equation (20) we expect a flux of

$$\frac{d^2N_\gamma}{dA\,dt}(>100\text{ TeV}) < 3\times10^{-16}\text{ cm}^{-2}\text{ s}^{-1} \qquad (23)$$

from the PBH background. This flux is unfortunately below the flux expected from galactic cosmic rays interacting with the interstellar medium (ref. 19; and F.H., J.H.M., T.C.W. and E.Z., in preparation). Note, however, that the lifetime of a 10 TeV black hole is ~1 s (see equation (7)), and therefore our previous discussion of the final stages of black holes is also relevant here.

Detection and bounds

Ground-based γ-ray telescopes, which detect air showers initiated by photons of energy TeV to PeV (see Box 2), can be used to search for PBHs or to set limits on their density expiring in the present epoch. A revitalized search for PBHs has been prompted by the development of new atmospheric Čerenkov and air-shower array telescopes which can identify γ-ray showers amid the much greater background of charged cosmic rays, and by the more definite particle physics predictions for final evaporation discussed in the previous section. The proposed detection techniques are generally based on the same principles as before. Experimentally there are two fundamental considerations in such searches. First, how large a volume can the telescope search efficiently and for what exposure time? Second, what conclusively distinguishes individual PBH emissions from a chance coincidence of background cosmic-ray showers?

At 100 TeV energies, experiments are being commissioned with collection areas in excess of 10^{10} cm^2 and angular resolutions less than 4×10^{-4} sr (ref. 35). Hadron rejection ratios,

TABLE 1 Summary of γ-ray flux at energies above E_D

$\Delta\tau$	10^6 s	10^3 s	1 s
$N_\gamma[>E_D, \tau<\Delta\tau]$	4.4×10^{31}	4.8×10^{30}	2.2×10^{29}
$\frac{dN_\gamma(>E_D)}{dt}$	1.0×10^{25} s^{-1}	2.5×10^{27} s^{-1}	1.3×10^{29} s^{-1}

TABLE 2 Observational limits on PBH densities

Technique*		Group†	Assumptions‡	Density of events (pc^{-3} yr^{-1})	References
ACT	3×1.5 m	SAO–UCD	HM	<0.47	Ref. 44
ACT	10 m	SAO–UCD	HM	<0.67	Ref. 44
ACT	4×1.5 m	SAO–UCD	HM	<2.1	Ref. 45
ACT	10 m+9 m	SAO–UCD	HM	<0.04	Ref. 45
ACT	10 m	SAO–UCD	EPM	$<7\times10^{5}$	Ref. 45
ACT	10 m	SAO–UCD	EPM	$<8\times10^{5}$	Ref. 46
ACT	2×1.5 m	SAO–UCD	EPM	$<3\times10^{4}$	Ref. 46
ACT	10 m	SAO–UCD	EPM	$<2\times10^{4}$	Ref. 47
EAS	2 arrays	UCC–UCD	EPM+UHE emission	$<2\times10^{4}$	Ref. 48
EAS	1 array	Tata	EPM+UHE emission	$<3\times10^{3}$	Ref. 49
Optical	3×1.5 m	UCD	EPM+optical emission	<0.3	Ref. 50
Radio	10 m	SAO	EPM+radio emission	$<3\times10^{-7}$	Ref. 51
Radio			EPM+radio emission	$<2\times10^{-7}$	Ref. 52
Radio	Arecibo	U. Mass	EPM+radio emission	$<7\times10^{-10}$	Refs 53–55

* ACT: atmospheric Cerenkov technique; EAS: extensive air shower.
† SAO: Smithsonian Astronomical Observatory; UCD: University College Dublin.
‡ HM: Hagedorn model; EPM: elementary particle model or standard model; UHE: ultra-high-energy.

based on the muon-to-electron ratio, of 10^{-4}–10^{-5} (ref. 37) are expected, although this has yet to be demonstrated in the detection of a discrete source. Air-shower arrays are now being discussed with lower energy thresholds in the 10–100 TeV range[37,38]. As an illustration, let us consider a somewhat idealized air-shower array telescope with the following parameters: collection area $A_D = 10^8$ cm^2, angular resolution $\omega_D = 4\times10^{-4}$ sr, energy threshold $E_D = 10$ TeV, operation time 1 year and hadron rejection ratio 10^{-3}. We will assume a typical zenith angle cutoff of 30°, and hence an acceptance angle of $\omega_A = 0.75$ sr. The depth of sky covered by the telescope can be calculated from the minimum flux sensitivity for detection of a burst. If n_γ is the minimum number of γ-rays of energy $>E_D$ required to register as a burst, then

$$n_\gamma = \frac{A}{4\pi r^2} N_\gamma(>E_D) \tag{24}$$

where r is the distance to the PBH. From equation (7), both extensive air-shower arrays and Čerenkov telescopes become sensitive to the direct photon flux from a black hole at a time

$$\Delta\tau \leqslant \left[\frac{5\times10^{13}\ \text{g GeV}}{E_D}\right]^3 \frac{1}{3\alpha(M)} \tag{25}$$

before the hole completely evaporates. The relevant emission period, $\Delta\tau$, is very sensitive to the detector threshold E_D. If $E_D = 10$ TeV, then $\Delta\tau \approx 64$ s, which in turn fixes the black-hole temperature and the peak photon energy Q for this detector. The hole emits a total flux of $\sim5.7\times10^{27}$ photons above threshold in the last 74 s; see equation (16). Of this flux, 77% is emitted in the last second. If we require a signal of n_γ photons within $\Delta\tau = 1$ s, and within the detector resolution, the depth of sky scanned by the detector is

$$r_\gamma \approx 0.035 \sqrt{\frac{A}{10^8\ \text{cm}^2}\frac{3}{n_\gamma}}\ \text{pc} \tag{26}$$

For the above values, $r_\gamma = 0.035$ pc, giving a scanned volume of $V_\gamma = \omega_A r^3/3 = 1.1\times10^{-5}$ pc^3.

The relevant background for our search comes from hadronic cosmic rays with energy close to E_D. The background rate of cosmic-ray showers is

$$\frac{d^3N_{cr}}{dA\,dt\,d\omega}(>E_D) = 0.21\left[\frac{E}{1\ \text{GeV}}\right]^{-1.5}\ \text{cm}^{-2}\,\text{s}^{-1}\,\text{sr}^{-1} \tag{27}$$

For $E_D = 10$ TeV and $\omega_D = 10^{-3}$ sr, the telescope would see a background of 0.02 s^{-1} per resolution element. If the rejection ratio is 10^{-3}, the minimum detectable photon event rate is then 2×10^{-5} s^{-1} per resolution element. For $n_\gamma = 3$ and $\Delta\tau = 1$ s, the chance of cosmic rays mimicking individual PBH emission from any direction is $<10^{-4}$ yr^{-1}. If no bursts were detected in one year of operation, we could set a limit of 4.3 events yr^{-1} at the 99% confidence level in V_γ. This would lead to an upper limit on the PBH explosion density of $dn/dt \leqslant 3.9\times10^5$ yr^{-1} pc^{-3}.

An alternative approach is to use atmospheric Čerenkov telescopes. These have considerably lower E_D and much smaller fields of view than air-shower arrays and must be operated under clear dark skies. Sophisticated detectors can reject background hadronic cosmic rays with 99% efficiency using differences in the Čerenkov images from hadronic and photonic air shows[39]. To evaluate the PBH detection efficiency, we consider the GRANITE telescope[40], now under construction at the Whipple Observatory. It consists of two 10-m-aperture optical concentrators, each fitted with a 109-pixel electronic camera, and separated by 120 m. The telescope is triggered by coincidences between corresponding pixels in the two concentrators. The energy threshold for γ-ray shower detection is 100 GeV, the full field is 2.5° ($\omega_A = 1.4\times10^{-3}$ sr), the angular resolution is of the order of the pixel size, 0.25°, and the collection area is $A_D = 5\times10^8$ cm.

Lower thresholds imply sensitivity to the larger fluxes resulting from jet fragmentation, and hence larger probed depths. This compensates for the reduced field of view so that their sensitivity is comparable to extensive air-shower arrays. Table 1 summarizes the flux and time-integrated flux, above E_D, as estimated from equations (16) and (17). For example, for small zenith angles and $\Delta\tau = 1$ s, the probed depth is $r_\gamma \approx 0.48$ pc and the sensitive volume is $V_\gamma \approx 5.2\times10^{-5}$ pc^3. The sensitivity can be further improved by exploiting the unusual zenith angle variation of Čerenkov telescopes. Simulations[41] show that as zenith angle increases, E_D and A_D increase by a factor f. At a zenith angle of 75°, we have $f = 100$. In this case, $A_D = 5\times10^{10}$ cm^2 and $E_D = 10$ TeV, which, for $n_\gamma = 4$, gives $r_\gamma \approx 0.72$ pc and $V_\gamma \approx 1.7\times10^{-4}$ pc^3.

The background of cosmic-ray events comes from distant proton showers of similar energies which arrive nearly parallel to the telescope's optical axis and from more local showers which traverse both telescopes' fields of view and radiate into the cone of the cameras. The former is estimated at 0.0015 s^{-1} pixel^{-1} for a rejection ratio of 10^{-2}. The latter can be rejected by examining the images. An observing time of 1,000 h in a dedicated experiment and $n_\gamma = 3$ will give a chance of <0.01 of mimicking a PBH. If no events are found in this time, then an upper limit on the number of PBH explosions of $\leqslant 1.3\times10^5$ yr^{-1} pc^3 for $V_r = 3\times10^{-4}$ pc^3 can be inferred. This is weaker

than the limit obtained from the MeV bound assuming maximum clustering given in equation (14).

In the alternative model with an exponentially growing number of degrees of freedom, 6.0×10^{34} erg of energy is evaporated in a final burst lasting 10^{-7} s. A significant fraction of the emission will be γ-rays of average energy 250 MeV. In this case the volume scanned by a dedicated telescope is large enough to strengthen the MeV bound on Ω_{pbh} considerably. The most sensitive detectors are atmospheric Čerenkov telescopes which detect bursts as if they were large air showers. A burst of 250-MeV γ-rays strikes the top of the atmosphere like a plane wave and interacts to produce secondary electrons. These in turn cause the atmosphere to radiate Čerenkov light which reaches the detector. Several independent estimates suggest that each vertically incident 250-MeV γ-ray produces on average ~2,300 optical photons reaching detector level[37,42]. Although individual photons cannot be detected, the combined effect is equivalent to a giant shower of 100 ns duration. The challenge is to design a detector that can detect the weakest possible γ-ray flux (and hence be sensitive to the greatest possible depth) while at the same time maximizing the field of view (and hence the volume V_γ). The accidental trigger rate from background events (such as local air showers, night-sky fluctuations and man-made sources) must be minimized to get maximum exposure time under clear, dark, night-sky conditions. In general, these conditions are not found in conventional atmospheric Čerenkov experiments, and the most sensitive measurements require specially designed experiments.

The most sensitive direct limit on the explosion rate (Box 3) was set by the operation of two large optical reflectors in coincidence in 1976 (ref. 42). In this experiment a cluster of phototubes was operated in coincidence with a 9-m optical reflector at the While Sands Missile Range and on a 10-m reflector at the Whipple Observatory, 400 km away. Both reflectors were pointed in the same direction under clear skies for 22.5 h; no coincidences were seen. The threshold for the detection of an event was 26 optical photons m^{-2}, giving a burst sensitivity of 5.6×10^{-10} erg cm^{-2}. For $E_B\approx10^{34}$ erg, this gave a maximum detectable distance of 390 pc, a sensitive volume of $V_\gamma = 4.4\times10^4$ pc^3 and in this model a limit on bursts of <0.04 pc^{-3} yr^{-1}.

Greater sensitivity could be achieved using the two 11-m aperture Solar concentrators at Sandia Labs, Albuquerque[43] together with the GRANITE telescopes (2×10 m)[40] now under construction at the Whipple Observatory in Arizona. Each reflector would be equipped with an array of phototubes to give a full field of view of 3°. A local coincidence would be demanded between each set of telescopes which would then be put in coincidence (by telephone link) with each other. The 100-ns duration of the pulses would be verified using waveform digitizers at each telescope (eliminating possible spurious events). With the increased collection area and a more sophisticated trigger, the threshold per burst could be reduced to 1.8×10^{-10} erg cm^{-2}, increasing V_γ by a factor of eight. The exposure time could also be increased to 450 h in six months of operation. A PBH limit as low as 2.5×10^{-4} explosions pc^{-3} yr^{-1} might then be obtained.

Results

Within the context of the standard model of quarks and leptons, we have discussed the signatures of black-hole evaporations and obtained a firm bound on the PBH abundance from MeV data. The standard model is incomplete, and new degrees of freedom should be revealed at yet higher energies. We have argued the possibility for improving the MeV bound by exploiting the new generation of TeV and PeV telescopes. Even in the absence of a detection, improvements of the bounds are a worthwhile endeavour as they provide direct information about the homogeneity and isotropy of the early Universe. □

F. Halzen and E. Zas are at the Department of Physics, University of Wisconsin, Madison, Wisconsin, USA. J. H. MacGibbon is at Code 665 NASA/Goddard Space Flight Center, Greenbelt, Maryland 20771, USA. T. C. Weekes is at the Whipple Observatory, Harvard Smithsonian Center for Astrophysics, P.O. Box 97, Amado, Arizona 85645-0097, USA.

BOX 3 Previous searches for PBH γ-ray bursts

Several direct experimental searches for PBH explosions were made in the 1970s following the theoretical discovery of PBH evaporation. In general, these involved the use of ground-based γ-ray telescopes and used both archival data and observations made with specially configured detectors. No statistically significant detection was reported, but upper limits were derived that placed limits on the PBH density.

Two extreme models for the final stages of the evaporation were considered, each predicting quite different parameters for the γ-ray burst. The experiments were confined to searches for bursts with these characteristics. The standard model (also known as the elementary particle model or EPM) predicted an outburst of 10^{30} erg in γ-rays of energy 5 TeV, lasting 0.1 s. The Hagedorn model, which corresponds to the exponential model discussed in the text, predicted an outburst of 10^{34} erg in 250 MeV γ-rays, lasting 100 ns.

In addition, it was postulated[50-55] that under certain conditions the exploding PBH might produce detectable radio or optical emission. In this scenario, the final e^+e^- emission from the PBH is braked by an ambient magnetic field as the particle shell expands relativistically away from the hole, thus producing an electromagnetic pulse. The pulse would only be appreciable if the explosion is governed by the Hagedorn model—a conclusion strengthened by the most recent analysis including quark and gluon emission[12]. Because of the greater sensitivity of radio and optical techniques, it was possible to probe greater depths with these experiments. A null result in these searches had less force, however, as the conditions for pulse production are highly model-dependent.

In Table 2 we list the principal searches that have been made, the techniques and assumptions used and the limits derived on the number density of PBHs; see refs 44-55. The latter show a spread of 10^{14}.

1. Carr, B. J. in *Observational and Theoretical Aspects of Relativistic Astrophysics and Cosmology* (eds Sanz, J. L. & Goicoechea, L. J.) 1-78 (World Scientific, Singapore, 1985).
2. Hawking, S. W. *Mon. Not. R. astr. Soc.* **152,** 75-78 (1971).
3. Hawking, S. W. *et al. Phys. Rev.* D**26,** 2681-2693 (1982).
4. Hawking, S. W. *Phys. Lett.* B**231,** 237-239 (1989).
5. Polnarev, A. & Zembowicz, R. *CAMK preprint 194* (1988).
6. Hawking, S. W. *Nature* **248,** 30-31 (1974).
7. Novikov, I. D. *et al. Astr. Astrophys.* **80,** 104 (1979).
8. Zeldovich, Ya. B. & Starobinskii, A. A. *Sov. Phys. JETP* **24,** 571 (1976).
9. Hall, S. J. & Hsu, S. *Berkeley preprint LBL-27982* (1989).
10. Carr, B. J. *Astr. J.* **206,** 8-25 (1976).
11. Page, D. N. & Hawking, S. W. *Astrophys. J.* **206,** 1-7 (1976).
12. MacGibbon, J. H. & Carr, B. J. *Astrophys. J.* **371,** 447-469 (1991).
13. MacGibbon, J. H. & Webber, B. R. *Phys. Rev.* D**41,** 3052-3079 (1990).
14. MacGibbon, J. H. *Phys. Rev.* (in the press).
15. Weekes, T. C. *Phys. Rep.* **160,** 1-121 (1988).
16. Bonnet-Bidaud, J. M. & Chardin, G. *Phys. Rep.* **170,** 325 (1988).
17. Protheroe, R. in *Proc. 20th ICRC, Moscow, 1987,* vol. 8 (ed. Kozyarivksy, V. A. *et al.*) (Nauka, Moscow, 1987).
18. Nagel, D. E., Gaisser, T. K. & Protheroe, R. J. *Ann. Rev. Nucl. Part. Sci.* **38,** 609-657 (1988).
19. Halzen, F., Protheroe, R. J., Stanev, T. & Vankov, H. P. *Phys. Rev.* D**41,** 342-346 (1990).
20. Halzen, F., Protheroe, R. J., Stanev, T. & Vankov, H. P. in *Proc. 21st ICRC, Adelaide* (ed. Protheroe, R. J.) (Adelaide University, 1990).
21. Page, D. N. *Phys. Rev.* D**13,** 198-206 (1976).
22. Page, D. N. *Phys. Rev.* D**16,** 2402-2411 (1977).
23. Elster, T. *J. Phys.* A**16,** 989-996 (1983).
24. Elster, T. *Phys. Lett.* A**92,** 205-209 (1983).
25. Simpkins, R. D. thesis, Pennsylvania State Univ. (1986).
26. Oliensis, J. & Hill, C. T. *Phys. Lett.* B**143,** 92-102 (1984).
27. Huang, K. & Weinberg, S. *Phys. Rev. Lett.* **25,** 895-897 (1970).
28. Hagedorn, R. *Nuovo Cim.* **LVIX,** No. 4, 1027-1057 (1968).
29. MacGibbon, J. H. thesis, Univ. of Cambridge (1988).
30. Carr, B. J. *Astrophys. J.* **201,** 1-19 (1975).
31. Hill, C. T., Schramm, D. V. & Walker, T. P. *Phys. Rev.* D**36,** 1007-1016 (1987).
32. Halzen, F., Stanev, T., Zas, E. & Gaisser, T. K. in *Proc. 21st ICRC, Adelaide,* vol. 9 (ed. Protheroe, R. J.) 142-145 (Adelaide University, 1990).
33. Trombka, T. I. *et al. Astr. J.* **212,** 925 (1977).
34. Fichtel, C. E., Simpson, G. A. & Thompson, D. J. *Astr. J.* **222,** 833 (1978).
35. Gibbs, K. J. *Nucl. Instr. Meth.* A**264,** 67-73 (1988).
36. Gaisser, T. K., Halzen, F., Long, W., Stanev, T. & Zas, E. *Phys. Rev.* D**43,** 314 (1990).
37. Sobel, H. *Nucl. Phys. B (Proc. Suppl.)* A**14,** 125-142 (1990).
38. Heintze, J., Lennert, P., Polenz, S. *et al. Nucl. Phys. B (Proc. Suppl.)* A**14,** 148-152 (1990).
39. Weeks, T. C. *et al. Astrophys. J.* **342,** 379-395 (1989).
40. Akerlof, C. W. *et al. Nucl. Phys. B (Proc. Suppl.)* A**14,** 237-243 (1990).
41. Sommers, P. & Elbert, J. in *Proc. 19th ICRC, 1985,* vol. 3, 457-460.

42. Porter, N. A. & Weekes, T. C. *Mon. Not. R. astrr. Soc.* **183,** 205–210 (1978).
43. Akerlof, C. W. *et al.* in *Proc. 21st ICRC, Adelaide,* vol. 2 (ed. Protheroe, R. J.) 135–138 (Adelaide University, 1990).
44. Porter, N. A. & Weekes, T. C. *Astrophys. J.* **212,** 224–226 (1977).
45. Porter, N. A. & Weekes, T. C. *Mon. Not. R. Astr. Soc.* **183,** 205–210 (1978).
46. Porter, N. A. & Weekes, T. C. *Nature* **277,** 199 (1979).
47. Nolan, K., Porter, N. A., Fegan, D. J., Chantell, M. & Weekes, T. C. *Proc. 21st ICRC, Adelaide,* vol. 2 (ed. Protheroe, R. J.) 150 (Adelaide University, 1990).
48. Fegan, D. J., McBreen, B., O'Brien, D. & O'Sullivan, C. *Nature* **271,** 731–732 (1978).
49. Bhat, P. N. *et al. Nature* **284,** 433–434 (1984).
50. Porter, N. A. & Weekes, T. C. *Nature* **267**, 500–501 (1977).
51. O'Mongain, E. *Nature* **242,** 136–137 (1973).
52. Huguenin, G. R. & Moore, E. L. *Astrophys. J.* **187,** L57–L58 (1974).
53. Phinney, S. & Taylor, J. H. *Nature* **277,** 117–118 (1979).
54. Rees, M. J. *Nature* **266,** 333–334 (1977).
55. Jelley, J. V., Baird, G. A. & O'Mongain, E. *Nature* **267**, 499–500 (1977).

ACKNOWLEDGEMENTS. We thank C. J. Goebel for giving his time whenever we needed expert help. We thank N. Porter for discussions. This research was supported in part by the University of Wisconsin Research Committee with funds granted by the Wisconsin Alumni Research Foundation, in part by the US Department of Energy, in part by the Xunta de Galicia (Spain) and in part by the Smithsonian Scholarly Studies Research Fund. J.H.M. is a NAS/NRC research associate.

ARTICLES

Crystal structure of insecticidal δ-endotoxin from *Bacillus thuringiensis* at 2.5 Å resolution

Jade Li*, Joe Carroll† & David J. Ellar†

* Medical Research Council Laboratory of Molecular Biology, Hills Road, Cambridge CB2 2QH, UK
† Biochemistry Department, Cambridge University, Tennis Court Road, Cambridge CB2 1QW, UK

The structure of the δ-endotoxin from *Bacillus thuringiensis* subsp. *tenebrionis* that is specifically toxic to Coleoptera insects (beetle toxin) has been determined at 2.5 Å resolution. It comprises three domains which are, from the N- to C-termini, a seven-helix bundle, a three-sheet domain, and a β sandwich. The core of the molecule encompassing all the domain interfaces is built from conserved sequence segments of the active δ-endotoxins. Therefore the structure represents the general fold of this family of insecticidal proteins. The bundle of long, hydrophobic and amphipathic helices is equipped for pore formation in the insect membrane, and regions of the three-sheet domain are probably responsible for receptor binding.

THE δ-endotoxins are a family of insecticidal proteins produced by *Bacillus thuringiensis* (B.t.) during sporulation, having relative molecular masses (M_r) 60,000–70,000 (60K–70K) in the active form and specific toxicities against insects in the orders of Lepidoptera, Diptera and Coleoptera[1,2]. These toxins have been formulated into commercial insecticides for three decades[3], and now insect-resistant plants are engineered by transformation with Lepidoptera-specific toxin genes[4–6]. In the bacterium δ-endotoxins are synthesized as protoxins of M_rs 70K–135K and crystallize as a parasporal inclusion ~1 μ in size, in which form they are ingested by the susceptible insect. The microcrystal dissolves in the alkaline pH of the midgut and the protoxin is cleaved by gut proteases to release the active toxin. δ-Endotoxins activated *in vitro* bind specifically and with high affinity ($k_D \approx$ 0.1–20 nM) to protein receptors on brush-border membrane vesicles derived from the gut epithelium of target insects[7–9] and create leakage channels of 10–20 Å diameter in the cell membrane[10]. *In vivo* such membrane lesions lead to swelling and lysis of the gut epithelium[11] and death of the insect ensues through starvation and septicaemia. Active δ-endotoxins of different specificities show five strongly conserved regions in their amino-acid sequences[1,12]. Exchanging sequence segments in the divergent regions between toxins of different specificities can produce active hybrids showing altered target specificity[13–15]. We have determined the atomic structure of a Coleoptera-specific δ-endotoxin (CryIIIA, beetle toxin) from *B.t.* subsp. *tenebrionis*[16–18] to elucidate the structural basis for target specificity and membrane perforation by this family of proteins.

Structure determination

Parasporal crystals of the beetle toxin contain the full-length 644-residue protoxin[17] as the minor component, and a product of bacterial processing with 57 residues removed from the N-terminus as the major component[19]. The latter (M_r 67K) is similar in sequence to the active form of other δ-endotoxins. After solubilization, papain cleavage converts the mixture to the 67K toxin (see legend to Table 1). This was recrystallized in the original crystal form of the parasporal crystals, space group $C222_1$ and cell dimensions 117.1 by 134.2 by 104.5 Å, containing one molecule per asymmetric unit and 55% solvent by volume[18].

Initial evaluation of derivatives was carried out at 4.5 Å resolution with data collected on the FAST TV diffractometer[20] using CuKα radiation. Complete datasets (Table 1) were then collected to 2.5 Å resolution from native crystals using the imaging plate systems at the EMBL outstation at DESY and from the mercury and platinum derivatives on film at SRS Daresbury. The electron density map (Fig. 1) at 2.5 Å resolution calculated with phases from multiple isomorphous replacement (mean figure of merit, 0.63) was easily interpretable and was improved by solvent flattening[21,22]. A continuous polypeptide chain from residue 61 to residue 644 at the C terminus was traced unambiguously, and most side-chain atoms could be located in the map. The atomic model was built using the graphics program O (ref. 23) and had an initial *R*-factor of 37% for all data to 2.5 Å. After preliminary refinement using the program X-PLOR (ref. 24), the current model, containing 584 amino acid residues and 40 bound water molecules, has an *R*-factor of 19.9% and r.m.s. bond length deviation of 0.017 Å.

Description of the structure

Overview. The beetle toxin is a wedge-shaped molecule with a radius of gyration of 58 Å. As shown in Fig. 2*a*, it comprises three domains. Domain I, from the N terminus of the 67K toxin to residue 290, is a seven-helix bundle in which a central helix is completely surrounded by six outer helices tilted at about +20° to it (Fig. 3*b*,*c*). Domain II, from residues 291 to 500, contains three antiparallel β sheets packed around a hydrophobic core with a triangular cross-section (Fig. 4). Domain III, from residues 501 to 644 at the C terminus is a sandwich of two antiparallel β sheets (Fig. 5). Domains I and III make up the